Hindawi
Shock and Vibration
Volume 2023, Article ID 5541196, 11 pages
https://doi.org/10.1155/2023/5541196

Research Article

Analysis of Dust Reduction Characteristics of Multistage Tandem Dust Removal System

Jiajun Zhang, Dong Liang, and Yuanwen Cao

School of Mechatronics and Vehicle Engineering, Chongqing Jiaotong University, Chongqing 400074, China

Correspondence should be addressed to Dong Liang; cqjtuliangdong_me@163.com

Received 17 January 2023; Revised 7 May 2023; Accepted 29 May 2023; Published 15 June 2023

Academic Editor: Traian Mazilu

Asphalt hot regeneration pavement maintenance vehicle is a type of in situ heating waste asphalt special vehicle equipment for mix and regeneration of aged asphalt. When waste asphalt mixture is heated and melted, a lot of organic fumes are typically produced, along with dust from the mixing process. Because of the complex composition of the exhaust gases produced by asphalt hot regeneration pavement maintenance vehicles, it can be difficult to purify and remove them using a single method. In order to effectively purify exhaust gas with complicated compositions, a multistage combined treatment dust removal system structure is presented that includes cyclone sections, spray sections, and adsorption sections. With an emphasis on the cyclone section structure with the dust-gas separation function, computational fluid dynamics (CFD) is used to analyze the internal flow field characteristics, turbulence intensity, tangential velocity, and velocity field vector characteristics. The results reveal that the more symmetrical the distribution of tangential velocity field and static pressure field is, the greater the cyclone dust collector's dust removal efficiency is, the more stable the flow field is, and the lower the turbulence intensity is. Furthermore, the center cyclone's growing speed is adversely connected with dust removal effectiveness. As a result, an antiventuri cyclone dust collector with a scrambling column was designed. When the inlet air speed is 6 m/s, the dust removal efficiency of the improved device is 97.0%, which is 5.1% higher than that of the original device, and when the inlet air speed is 8 m/s, the dust removal efficiency of the improved device is 97.3%, which is 4.16% higher than that of the original device. With the increase of the inlet air speed, the difference between them keeps decreasing.

1. Introduction

Affected by material aging, severe weather, and highway loading, the asphalt layer of the asphalt pavement often develops various early damages such as ruts, cracks, and potholes within the design life [1]. These damaged pavements reduce vehicle safety and driving comfort. The asphalt thermal regeneration pavement maintenance vehicle can heat the waste asphalt from a damaged pavement in place to swiftly repair it and extend its service life, while reducing maintenance costs and waste of raw materials [2]. During the heating and melting process, however, waste asphalt will produce a significant amount of organic waste gas, as well as a significant amount of dust. The organic waste gas has a complex composition, mainly consisting of nitrogen oxides, sulfur oxides, polycyclic aromatic hydrocarbons, and other substances, and also contains strong carcinogens such as benzopyrene, carbazole, and anthracene derivatives, which pose a serious threat to the environment and the health of residents [3]. Therefore, special dust removal and exhaust gas purification systems must be designed for it.

There are few studies focused on vehicle-mounted systems for removing asphalt exhaust dust. Xu and Liu [4] conducted a study on particle agglomeration in low-temperature dust collectors and found that the lower the inlet flue gas temperature of the dust collector, the more obvious the particle agglomeration phenomenon is. Alizadehyazdi et al. [5] used an electrostatic dusting device to remove dust particles from the adhesive surface, which is optimized to be more effective than the usual rinsing means. Mo et al. [6] proposed a dust removal technology for a coal cutting machine with the car to solve the problem of dust

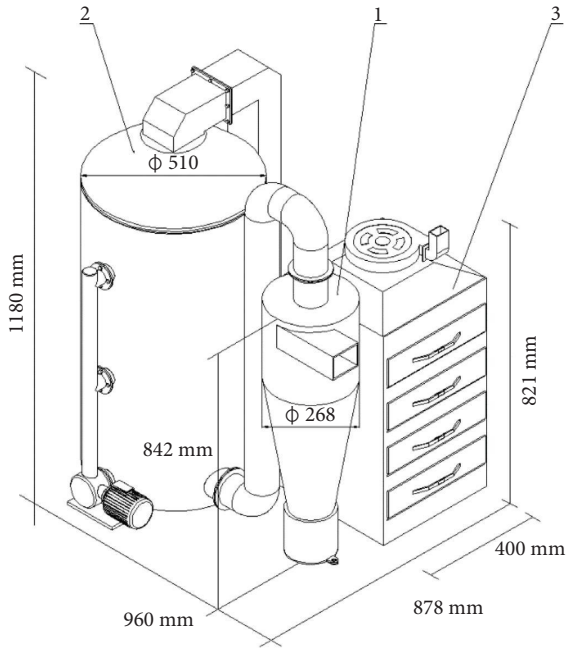

Figure 1: Structure diagram of the dust removal system: (1) cyclone section; (2) sprinkler section; (3) activated carbon adsorption section.

generated from the surface coal mining. A small dust collector is installed at the end of the coal cutter to prevent dust from spreading to the walkway side causing environmental pollution. Yi et al. [7] provided treating phenyl-containing organic waste gases with a surfactant absorbent solution. Yoshida et al. [8] investigated the rotational velocity distribution inside a dual inlet and single inlet dust collector. The data analysis showed that the rotational velocity distribution inside the multiple inlet dust collector is more uniform and symmetrical, thus effectively reducing friction and decay of the internal cyclonic flow. The experimental results also show that the former has a higher separation efficiency than the latter. Utilizing the discrete conjugate approach, Elsayed [9] suggested a new flared exhaust pipe while optimizing the least pressure drop of the cyclone. When compared to the standard plain cyclone, the optimized cyclone saves 66 percent of the driving power. Hsiao et al. [10] investigated the cyclone separator's longitudinal and radial dimensional ratios and optimized the structure. It was discovered that raising the barrel's height might lengthen the period of particle rotation separation and boost the effectiveness of dust removal. Sgrott et al. [11] performed simulation optimization of a cyclone dust collector by using CFD software for 5 μm to 15 μm dust simulation. Wang et al. [12] designed a new two-stage on-line gas-liquid cyclone separator. It integrates the advantages of horizontal and vertical inline gas-liquid cyclone separator, and it can meet the separation requirement for both gas and liquid. The tangential velocity, gas volume fraction, and pressure distribution inside the separator are studied by numerical simulation using computational fluid dynamics. In terms of numerical solution, Gopalakrishnan et al. [13] numerically

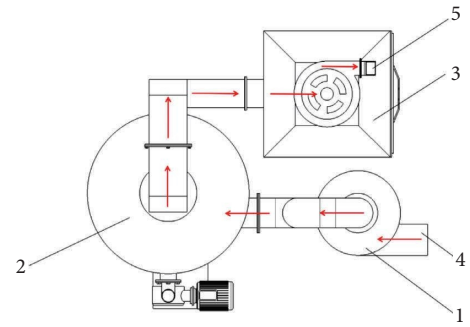

Figure 2: Air flow direction of the dust removal system: (1) cyclone section; (2) spraying section; (3) activated carbon adsorption section; (4) inlet; (5) exhaust.

investigated the particle separation through an axial vortex tube cyclone separator by solving the Reynolds-averaged Navier–Stokes equations using the RNG K-epsilon model as a discrete phase model (DPM) for turbulent closure and particles using the Eulerian–Lagrangian method. Yamasaki et al. [14] performed a multiobjective optimization of an axial cyclone separator to improve the overall performance at different velocities. The separation efficiency and pressure drop are taken as the objective functions.

This study offers a structural design for a dust removal system with multistage combined treatment to address the issue that it is challenging to purify asphalt fumes by a single method. It includes a cyclone section, a spraying section, and an adsorption section and achieves efficient purification of complex composition exhaust gases by the multistage sectional treatment.

2. Materials and Methods

2.1. New Multistage Combined Dust Removal System. The overall length, width, and height is 960 mm × 878 mm × 1180 mm, and the size of the arrangement space on the car is 1300 mm × 900 mm × 1600 mm. The structure of the dust removal system is depicted in Figure 1, which includes a cyclone section, a spraying section, and an activated carbon adsorption section.

Due to the special cone-shaped structure of the cyclone section separator, the airflow changes from linear to high-speed rotational motion after the gas enters through the air inlet. The dust particles are thrown against the cylinder wall by centrifugal force much greater than their own gravity, eventually settling in the dust collection box at the bottom of the cyclone dust collector.

Figure 2 shows the air flow diagram of the dust removal system. The exhaust gas enters the spray section after being pretreated in the cyclone section, which is connected to the spray section by a pipe. The spraying tank, spraying pipeline, pumping machine, and mist elimination plate are all parts of the spraying portion. To absorb sulfide in the exhaust gas, the alkaline liquid stored in the spray tank is circulated and sprayed in the spray tank via the pump machine and spray pipeline. The spraying portion is connected to the activated carbon adsorption section by a pipeline, and the activated

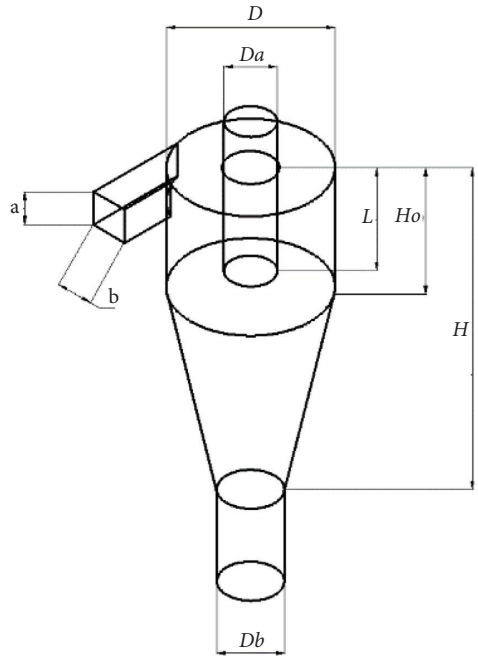

Figure 3: Cyclone separator structure schematic diagram.

carbon adsorption tank is filled with honeycomb activated carbon for adsorbing powerful carcinogenic compounds. The top of the activated carbon adsorption section has a centrifugal fan for suction.

2.2. Geometric Model of Cyclone Separator. The cyclone separator is an integral aspect of the asphalt waste gas pretreatment process for separating the gas-solid combination. Understanding the operating characteristics of the cyclone separator is crucial to improve the dust removal efficiency of the dust removal system. However, the flow field inside the cyclone section separator is complicated and variable, and the effects of various structures on separation efficiency and pressure drop are frequently interactive, making the experimental analysis difficult [15, 16]. As a result, this work uses numerical simulation to investigate the cyclone separator's internal flow field characteristics as a foundation for enhancing the structure.

Figure 3 is a schematic diagram of the structure of the cyclone separator, whose main structure includes inlet height a, inlet width b, barrel height *Ho*, total height *H*, exhaust pipe depth *L*, exhaust pipe diameter *Da*, barrel diameter *D*, and dust collection port diameter *Db*. The annular space is the cylindrical space of the cyclone section separator, the height of the annular space is *Ho*, the separation space is the conical space of the cyclone section separator, and the height of the separation space is *H-Ho*.

2.3. Numerical Simulation Methods

2.3.1. Selection of Mathematical Model. The flow field inside the cyclone separator is an extremely complex three-dimensional, gas-solid two-phase cyclonic flow with significant anisotropy, so the Reynolds Stress Turbulence Model (RSM) is selected for the analysis. The RSM model strictly considers the effects of flow line bending and vortices and has higher accuracy for complex turbulence simulations [17–19]. The RSM set of basic control equations for turbulence consists of the continuity equation, the N-S equation, the Reynolds stress equation, the turbulent kinetic energy equation, and the dissipation rate equation.

Assuming that the fluid in the cyclone section separator is incompressible and isothermal, the corresponding control equation is as follows.

Continuity equation is given by

$$\frac{\partial u_i}{\partial x_i} = 0. \tag{1}$$

Navier–Stokes equation is as follows:

$$\rho_g u_j \frac{\partial u_i}{\partial x_j} = -\frac{\partial p}{\partial x_j} + \frac{\partial}{\partial x_j}\left[\mu_g\left(\frac{\partial u_i}{\partial x_j} + \frac{\partial u_j}{\partial x_i}\right)\right] + \frac{\partial \tau_{ij}}{\partial x_j}, \tag{2}$$

where μ_g is the gas viscosity coefficient, ρ_g is the gas density, and τ_{ij} is the Reynolds stress term.

Reynolds stress transport equation is as follows:

$$\frac{\partial}{\partial x_k}\left(\rho_g u_k \overline{u_i' u_j'}\right) = D_{ij} + P_{ij} + \prod_{ij} - \varepsilon_{ij}, \tag{3}$$

where D_{ij} is the diffusive transport term, P_{ij} is the stress production term. $\prod_{ij}$ is the pressure-stress correlation term, and ε_{ij} is the dissipation term.

Turbulent energy equation is given by

$$\rho \frac{D_k}{D_t} = \frac{\partial}{\partial x_l}\left[\left(\frac{\mu_i}{\sigma_k} + \mu\right)\frac{\partial k}{\partial x_l}\right] - \rho \overline{u_i u_l}\frac{\partial U_i}{\partial x_l} - \rho\varepsilon. \tag{4}$$

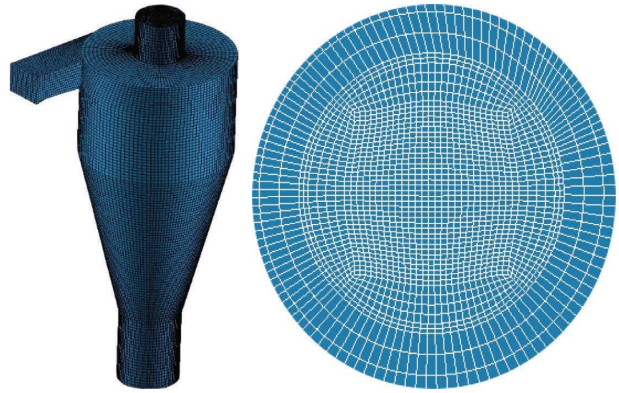

Figure 4: Structured mesh and O-block meshing details.

Dissipation rate equation is given by

$$\rho \frac{D_\varepsilon}{D_\tau} = \frac{\partial}{\partial x_l}\left[\left(\frac{u_l}{\sigma_k} + \mu\right)\frac{\partial \varepsilon}{\partial x_l}\right] - C_{\varepsilon 1}\frac{\varepsilon}{k}\frac{\mu_l}{2}\left(\frac{\partial u_i}{\partial x_j} + \frac{\partial u_j}{\partial x_i}\right)^2 - C_{\varepsilon 2}\rho\frac{\varepsilon^2}{k}, \tag{5}$$

where $C_{\varepsilon 1} = 1.44$ and $C_{\varepsilon 2} = 1.92$.

The arithmetic-saving DPM model [20–22] was chosen for the simulation of dust particles instead of treating the particles as one phase alone (VOF multiphase flow model). The cyclone separator has achieved 99% separation efficiency for the particles with diameters above 10 μm, and the dust particles simulated in this paper are 1 μm to 10 μm in diameter.

Using a QUICK differential format control discretization with second-order accuracy, the SIMPLE algorithm was employed to solve the coupled pressure-velocity equation [23]. The separation efficiency of the cyclone separator is calculated by the following equation:

$$N = 1 - \frac{\text{number of escaped particles}}{\text{number of captured particles}} \times 100\%. \tag{6}$$

2.3.2. Boundary Conditions. Inlet boundary conditions were as follows: velocity pressure inlet, inlet velocity 10 m/s, and hydraulic diameter 74.82 mm. Outlet boundary conditions were as follows: pressure outlet, pressure equal to standard atmospheric pressure, and hydrodynamic diameter 95 mm. Wall boundary conditions were as follows: no slip boundary conditions and particles are bounced after impact. The dust removal system was installed on the asphalt hot regeneration maintenance vehicle, and due to the on-board generator, there was a large degree of vibration during the actual operation, and the adhered particles would be shaken off. Therefore, in the numerical simulation, the wall was set to a mode where the particles would bounce back after collision. Capture failure occurs when dust particles pass through the outlet; capture success occurs when dust particles fall to the bottom of the dust collection box.

2.3.3. Mesh Division. All the meshes are structured, and the computational regions are divided by hexahedra. The details of cylindrical o-block meshing are shown in Figure 4. Keep encrypting the grid and observe the change of the result. When the number of grids reaches 425826, continuing to encrypt the grids has little effect on the results. At this time, the cloud map is smooth and continuous, and the results are highly credible. The calculation is mainly judged by the residual values of the iterations to determine whether the calculation converges or not. In addition, the judgment can be assisted by monitoring the mass flow rates of the inlet and outlet, and the calculation can be regarded as converging when the mass flow rates of the inlet and outlet reach equilibrium. In this paper, the residuals of the continuity equation and momentum equation are less than 10^{-4}, which can be regarded as the convergence of the computational model.

3. Results and Discussion

3.1. The Development Law of Internal Flow Field. Figures 5–7 show the cyclone section separator static pressure clouds, tangential velocity clouds, and turbulence intensity clouds at different exhaust pipe depths.

The simulation findings reveal that the static pressure in the cyclone's negative pressure zone increases with exhaust pipe depth and always emerges at the exhaust pipe's entrance. The negative pressure creates a pumping force that converts the cyclone's downward cyclonic flow into an upward cyclonic flow. The static pressure on both sides of the cyclone wall increases with the depth of the exhaust pipe, and the total pressure drop also increases.

The closer to the central column core, the lower the static pressure, and as the depth of the exhaust pipe increases, the core's static pressure distribution becomes more uniform and symmetrical. The tangential velocity cloud shows the same trend. The tangential velocity of the column core becomes more stable as the depth of the exhaust pipe increases, while velocity fluctuation decreases and the velocity of the updraft slows, making it more difficult for tiny particles to be carried away from the cyclone separator by the updraft, increasing the cyclone separator's dust and gas separation efficiency.

3.2. Device Improvement and Comparison. An antiventuri cyclone dust collector with a scrambling column is designed in Figure 8. The venturi has a narrow central portion and two

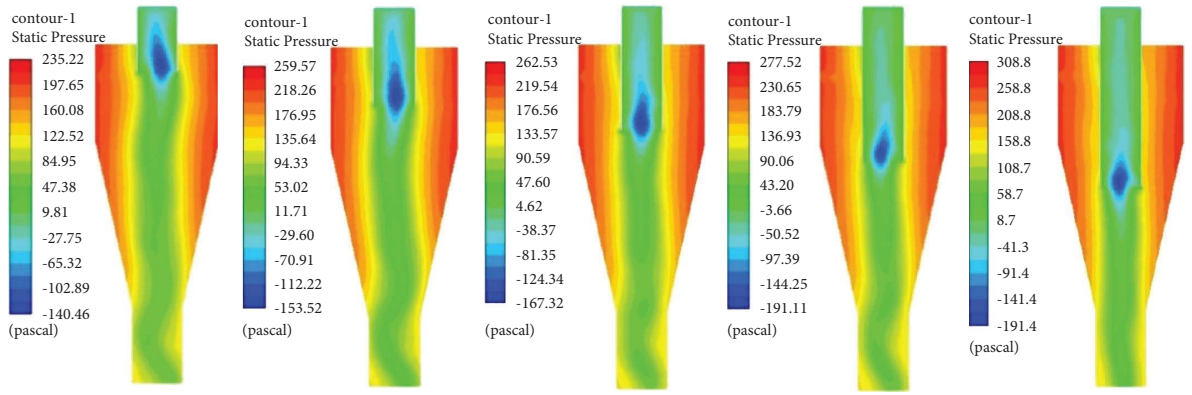

Figure 5: Static pressure cloud of an exhaust pipe with the depth of 75 mm, 150 mm, 225 mm, 300 mm, and 375 mm.

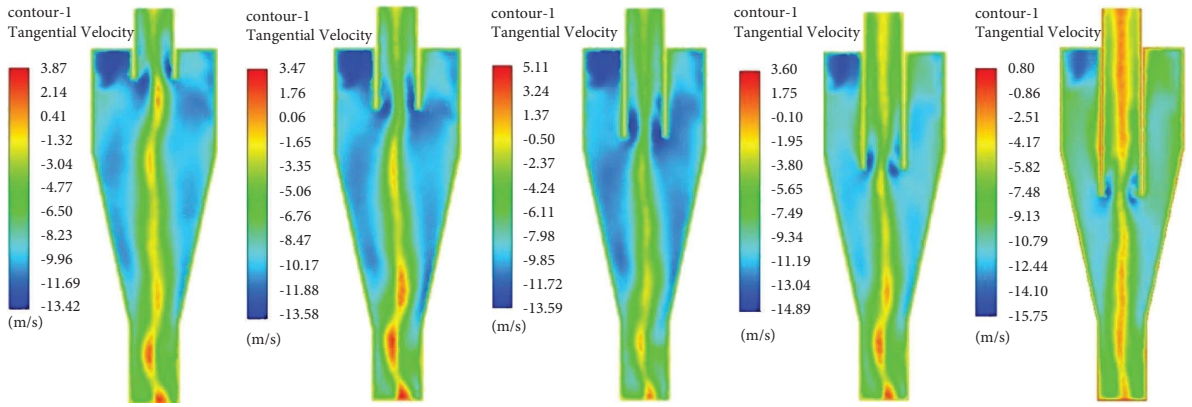

Figure 6: Tangential velocity cloud of an exhaust pipe with the depth of 75 mm, 150 mm, 225 mm, 300 mm, and 375 mm.

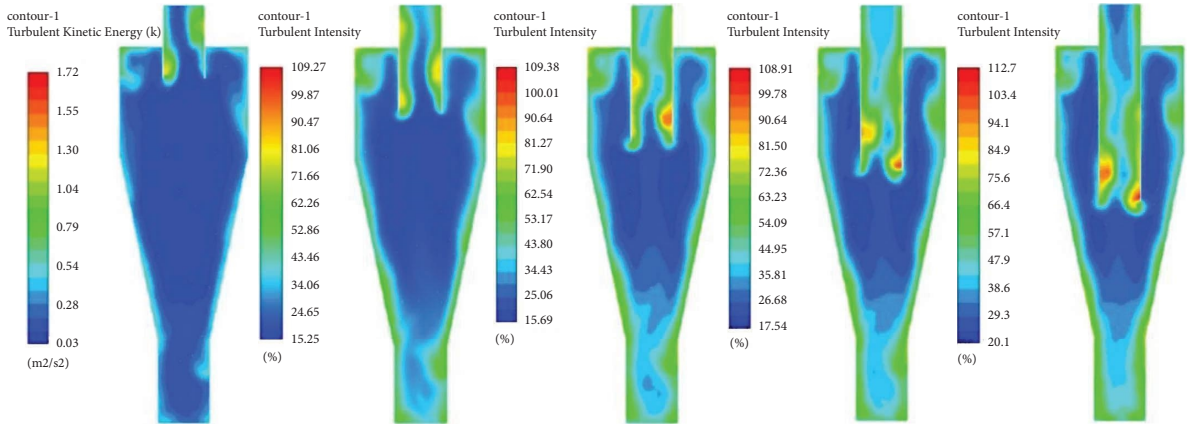

Figure 7: Cloud chart of turbulence intensity when the depth of an exhaust pipe is 75 mm, 150 mm, 225 mm, 300 mm, and 375 mm.

wide sections, which causes the airflow to change from coarse to thin, accelerates the airflow velocity, and creates a low pressure area at the venturi outlet's outer circle [24]. The middle of the antiventilator, on the other hand, is wide and the two sides are narrow, which has a retarding impact on the airflow and effectively reduces the rising speed of the airflow in the center of the cyclone dust collector under the same shape and size premise. The spoiler column at the bottom plays an important role in destroying the reverse cyclone there. The spoiler column forces the downward airflow to reverse ahead of time, avoiding pulling up fine dust particles that have accumulated at the bottom of the dust collector when it reverses at the bottom. This measure improves the efficiency of dust removal.

3.2.1. Comparison of Internal Flow Field Characteristics. Figure 9 shows the static pressure distribution cloud of the original and improved structures. Figure 9(a) shows the static pressure distribution of the original structure, and

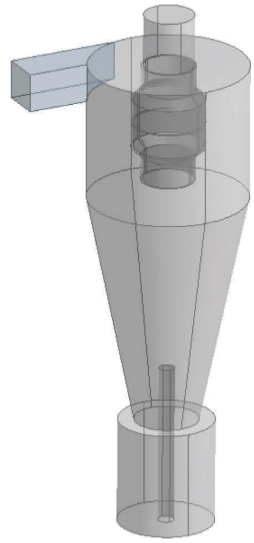

Figure 8: Structure diagram of the antiventuri cyclone with spoiler column.

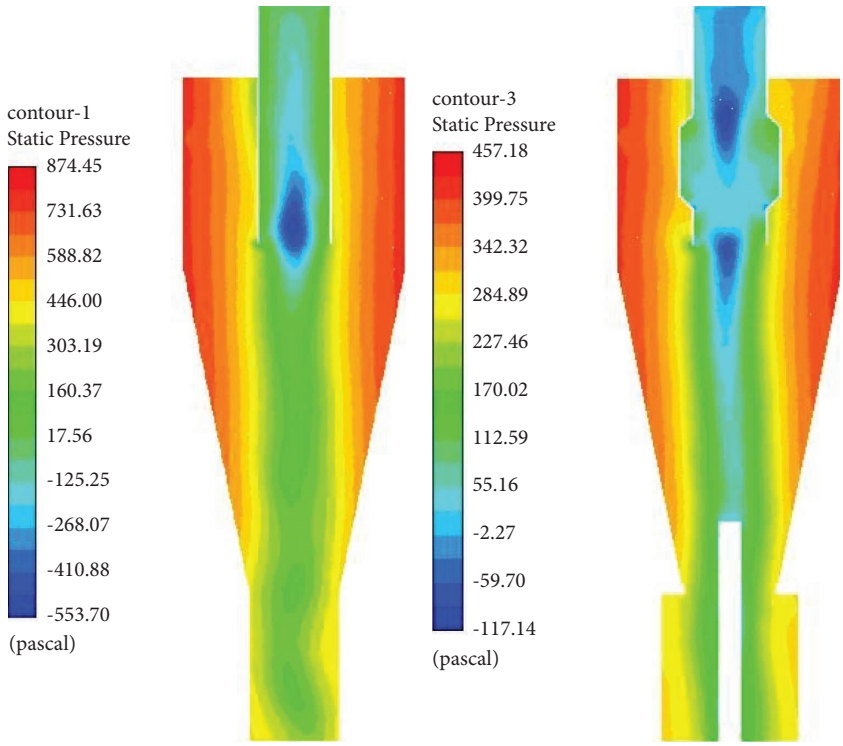

Figure 9: Static pressure distribution. (a) Original device. (b) Improved device.

Figure 9(b) shows the static pressure distribution of the improved structure. The simulation results show that compared with the ordinary cyclone with the same exhaust pipe depth, two negative pressure zones are formed inside the exhaust pipe of the antiventuri cyclone separator. The two negative pressure zones appear in the narrow section of the exhaust pipe, and the static pressure distribution is more symmetrical.

Figure 10 shows the tangential velocity distribution cloud of the original and improved structures, with Figure 10(a) being the original structure and Figure 10(b) being the improved structure. The local vortex at the bottom of the improved device is significantly reduced, and the maximum tangential velocity is 4.55 m/s, which is less than 9.74 m/s of the original device, and the updraft in the center of the device is more stable, which is conducive to improving

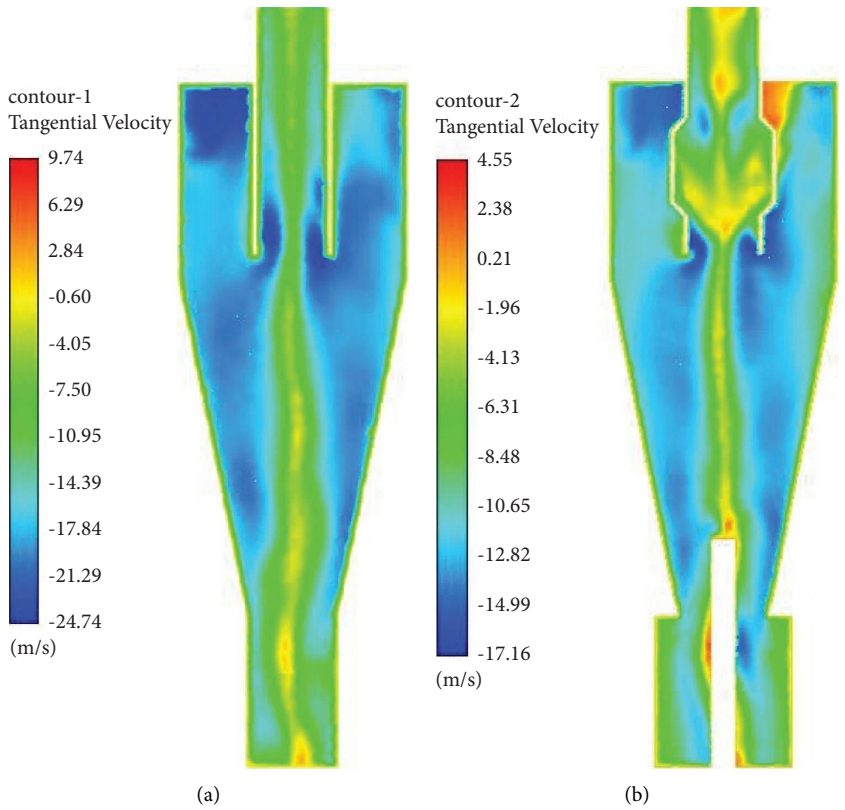

Figure 10: Tangential velocity distribution. (a) Original device. (b) Improved device.

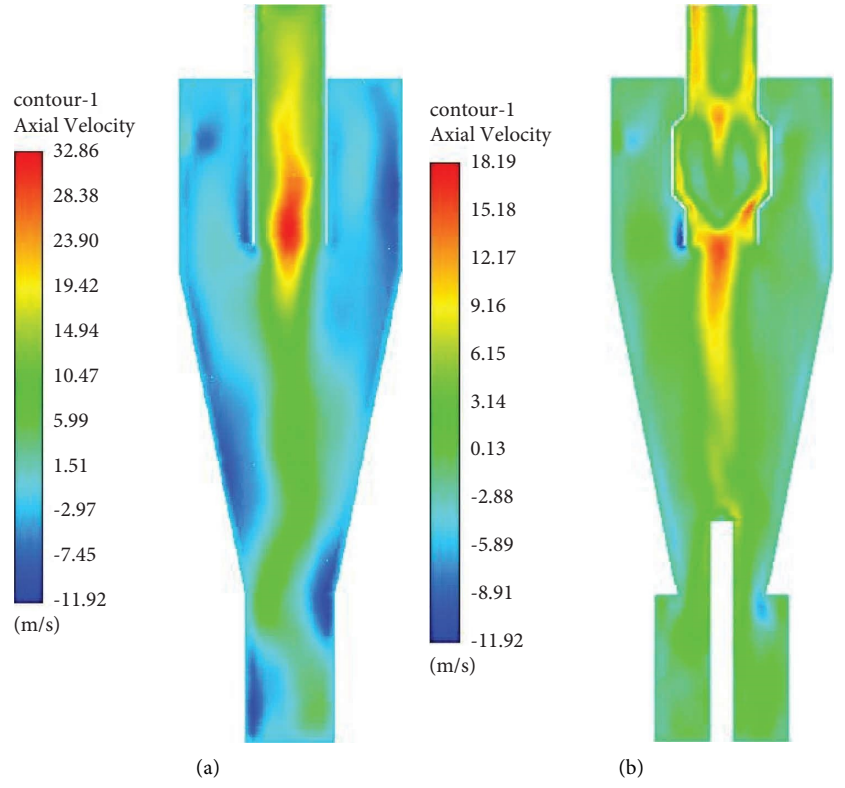

Figure 11: Axial velocity distribution. (a) Original device. (b) Improved device.

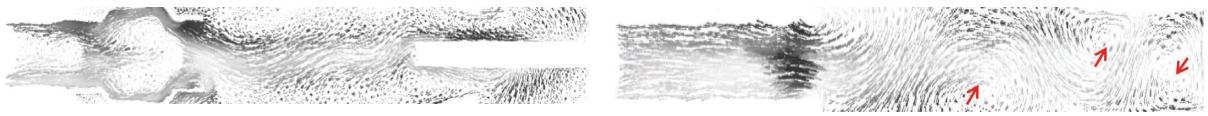

(a) (b)

Figure 12: Flow field trajectory diagram of the improved device and the original device.

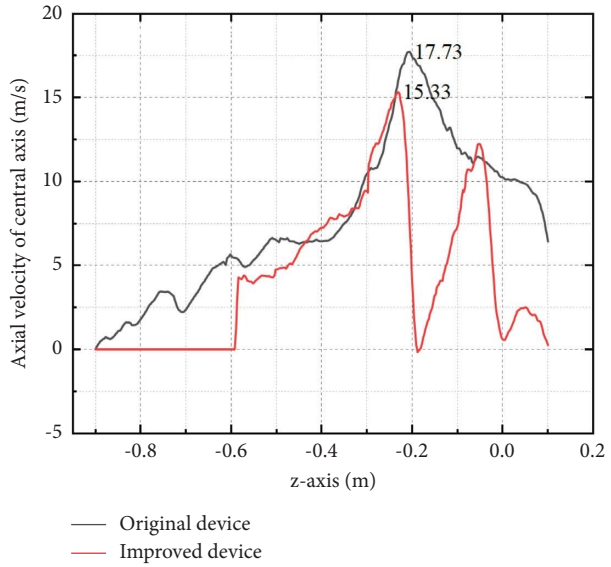

Figure 13: Diagram of the rise velocity of airflow in the center of the improved device and the original device.

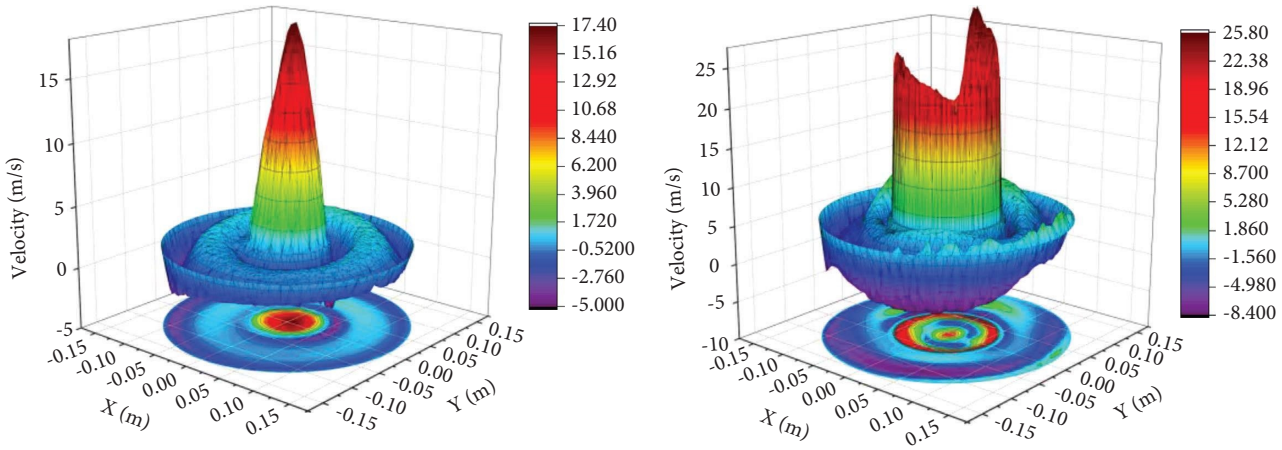

(a) (b)

Figure 14: $Z = 550$ mm height section airflow velocity diagram. (a) Original device. (b) Improved device.

the separation efficiency. Figure 11 shows the axial velocity distribution cloud of the original and improved structures, with Figure 11(a) being the original structure and Figure 11(b) being the improved structure. The axial velocity distribution can more specifically reflect changes in the upward velocity of the central airflow. In the original device, the reverse airflow from the bottom of the dust collector can easily develop into a local turbulent airflow, and in the improved device, this phenomenon is effectively suppressed.

3.2.2. Flow Field Trajectory Comparison. Figure 12 shows the velocity vector diagram of the air core of the improved device and the original device, the air core in the center of the improved device is smoother, while multiple turbulent

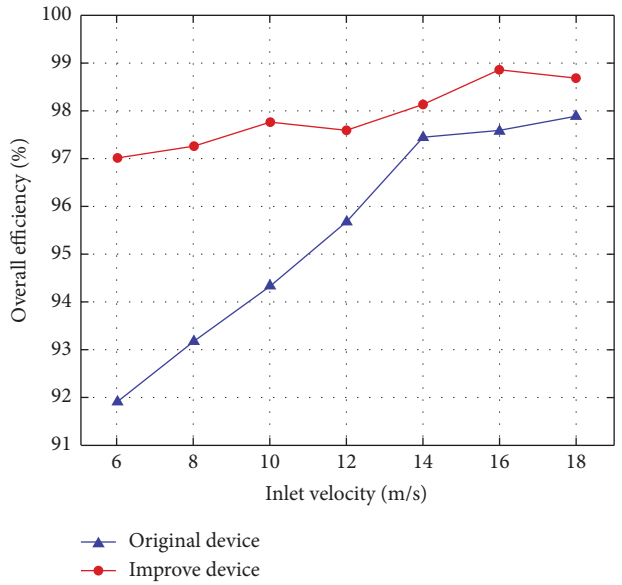

Figure 15: Total dust removal efficiency of the improved device and the original device at different air inlet speeds.

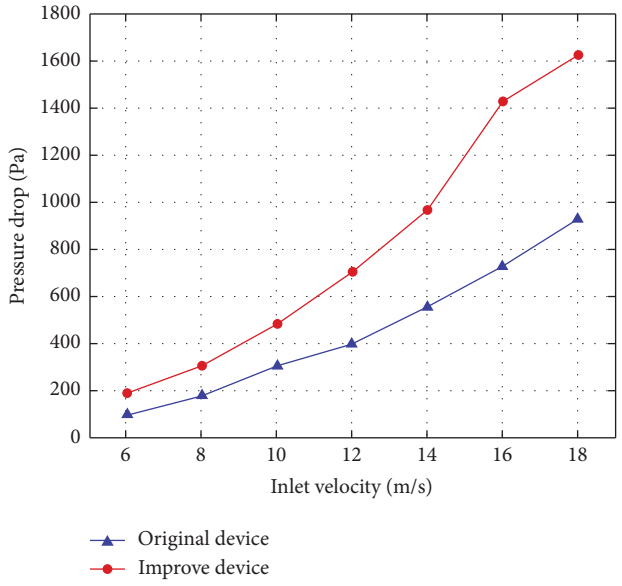

Figure 16: Total pressure drop of the improved device and the original device at different inlet speeds.

cyclones appear inside the original device. The bottom column has a clear influence on suppressing turbulent cyclones by causing airflow to move upward earlier, which should be reversed at the bottom.

3.2.3. Key Performance Comparisons. Figure 13 shows the axial rise velocity of the central airflow of the improved device and the original device, and the axial rise velocity of the central airflow of the improved device is 0 m/s in the range of −0.9 m–0.6 m because the bottom of the improved device is a solid column. The maximum axial rise speed of the improved device is 15.33 m/s, which is lower than 17.73 m/s result of the original device.

Figure 14 is a graph of airflow velocity at the same height cross section of the original device and the modified device, with the original device in Figure 12(a) and the modified device in Figure 12(b).

$Z = 550$ mm height section is located in the middle of the row pipe, and this position is the most representative of the full development of cyclones, stable flow velocity. Compared with the original device, the central cyclone of the improved device has a smaller rise velocity, and the maximum rise velocity of the central airflow of the original device is 17.3 m/s, while the maximum rise velocity of the central airflow of the improved device is 15.83 m/s. This is basically consistent with the data in Figure 11, which indicates that the central cyclone is significantly weakened in the improved device. The center cyclone will roll up the dust settled at the bottom during the rising process, causing the secondary entrainment phenomenon, and the smaller rising speed means that the dust at the bottom is more difficult to escape with the updraft.

The axial velocity of the two devices rises at the same rate at first, but when the airflow reaches the exhaust pipe, the upgraded device's maximum axial rise speed is substantially slower than the original device. In the exhaust pipe of the modified device, the airflow decelerates when passing through the flared section and accelerates when passing through the narrow section, and the total average velocity is less than that of the original device. At various inlet speeds, Figures 15 and 16 show the total dust removal efficiency and total pressure drop for the modified and original units.

The total dust removal efficiency of both the improved unit and the original unit increased with the increase of the inlet air speed, and the total dust removal efficiency of the improved unit was consistently greater than that of the original unit, which proved the advantage of the improved unit. When the air inlet speed is 6 m/s, the dust removal efficiency of the original device is 91.9%, and the dust removal efficiency of the improved device is 97.0%, which is 5.1% higher than the original device. When the air inlet speed is 8 m/s, the dust removal efficiency of the original device is 93.14%, and the dust removal efficiency of the improved device is 97.3%, which is 4.16% higher than the original device, and the difference between them keeps decreasing as the air inlet speed increases.

In addition, the difference between the two dust removal efficiencies decreases as the inlet air velocity increases. When the inlet speed is low, under 10 m/s, the total pressure drop of the improved device is slightly larger than that of the original device, but as the inlet speed rises, the total pressure drop of the improved device rises more quickly. For this reason, the inlet speed of the improved device should not be set too high. 2.

4. Conclusions

(1) This paper proposes a structural design method for the dust removal system of an asphalt hot regeneration pavement maintenance vehicle, using the concept of multistage combined treatment to complete the design of cyclone section, spraying section,

and adsorption section. The cyclone section uses a cyclone separator to remove dust particles from the exhaust gas; the spray section absorbs sulfides through circular spraying of lye; and the adsorption section adsorbs major carcinogens through honeycomb activated carbon.

(2) The CFD numerical simulation was used to analyze the structure of the cyclone section of the dust removal system, and the static pressure and tangential velocity inside the cyclone section were basically symmetrically distributed. The static pressure distribution and tangential velocity field inside the cyclone become increasingly symmetrical and stable as the depth of the exhaust pipe rises; the dust removal efficiency is positively related to the symmetry and stability of the flow field.

(3) A antiventilator cyclone with a scrambling column was designed. The venturi tube is narrow in the middle and wide at the ends, while the antiventuri tube is wide in the center and narrow at the ends. This design reduces the rising cyclone's speed and prevents the dust that has settled at the bottom of the dust collection tube from being raised once more, thus improving the dust removal efficiency. The presence of the scrambling column has a key role in suppressing the turbulent flow at the bottom of the cyclone, and the vortex eccentricity is significantly reduced or even eliminated, which makes the flow field inside the cyclone more stable.

(4) Further study on the experimental validation of the device will be carried out, including the construction of the prototype and experimental platform.

Data Availability

The data used to support the findings of this study are included within the article.

Conflicts of Interest

The authors declare that they have no conflicts of interest.

Acknowledgments

This work was supported by National Natural Science Foundation of China (Grant no. 52175042) and Chongqing Key Laboratory for Public Transportation Equipment Design and System Integration Open Fund (Grant no. CKLPTEDSI-KFKT-202102).

References

[1] F. X. Deng and Y. C. Zhu, "Research on construction technology of municipal road asphalt pavement with regeneration," *Traffic World*, vol. 582, no. 24, pp. 102-103, 2021.

[2] F. Y. Han, *Key Technology for Hot Regeneration of Old Asphalt Mixture in Cold Areas*, Chang'an University, Xi'an, China, 2020.

[3] T. Wang, *Study on the Fusion Behavior of Old and New Asphalt during thermal Regeneration*, Shandong Jiaotong University, Jinan, China, 2020.

[4] X. F. Xu and H. X. Liu, "Characterization of fly ash particle size in coal-fired power plants and research on particle agglomeration in low-temperature electric precipitators," in *Proceedings of The 18th China Academic Conference on Electrostatic Precipitation*, pp. 12–16, Electric Power Industry Press, Nanjing, China, 2019.

[5] V. Alizadehyazdi, M. Bonthron, and M. Spenko, "Optimizing electrostatic cleaning for dust removal on gecko-inspired adhesives," *Journal of Electrostatics*, vol. 108, no. 41, Article ID 103499, 2020.

[6] J. M. Mo, J. L. Yang, W. Ma, F. Chen, and S. Zhang, "Numerical simulation and field experiment study on onboard dust removal technology based on airflow–dust pollution dispersion characteristics," *Environmental Science and Pollution Research*, vol. 27, no. 2, pp. 1721–1733, 2020.

[7] X. Y. Yi, X. H. Zhao, and D. L. Zhu, "Pilot experiment of surfactant absorption method for the treatment of benzene containing exhaust gas," *Energy and Environmental Protection*, vol. 3, pp. 24–27, 2004.

[8] H. Yoshida, S. Yoshikawa, K. Fukui, and T. Yamamoto, "Effect of multi-inlet flow on particle classification performance of hydro-cyclones," *Powder Technology*, vol. 184, no. 3, pp. 352–360, 2008.

[9] K. Elsayed, "Design of a novel gas cyclone vortex finder using the adjoint method," *Separation and Purification Technology*, vol. 142, pp. 274–286, 2015.

[10] T. C. Hsiao, S. H. Huang, C. W. Hsu, C. C. Chen, and P. K. Chang, "Effects of the geometric configuration on cyclone performance," *Journal of Aerosol Science*, vol. 86, no. 8, pp. 1–12, 2015.

[11] O. L. Sgrott, D. Noriler, V. R. Wiggers, and H. F. Meier, "Cyclone optimization by complex method and CFD simulation," *Powder Technology*, vol. 277, no. 6, pp. 11–21, 2015.

[12] Q. Q. Wang, J. Q. Chen, C. S. Wang et al., "Design and performance study of a two-stage inline gas-liquid cyclone separator with large range of inlet gas volume fraction," *Journal of Petroleum Science and Engineering*, vol. 220, Article ID 111218, 2023.

[13] B. Gopalakrishnan, K. G. Saravana, and K. A. Prakash, "Parametric analysis and optimization of gas-particle flow through axial cyclone separator: a numerical study," *Advanced Powder Technology*, vol. 34, no. 2, pp. 211–223, 2023.

[14] H. Yamasaki, H. Wakimoto, T. Kamimura, K. Hattori, P. Nekså, and H. Yamaguchi, "Visualization and measurement of swirling flow of dry ice particles in cyclone separator-sublimator," *Energies*, vol. 15, no. 11, pp. 4128–4201, 2022.

[15] R. L. Salcedo, M. J. Pinho, and J. Pinho, "Pilot- and industrial-scale experimental investigation of numerically optimized cyclones," *Industrial & Engineering Chemistry Research*, vol. 42, no. 1, pp. 145–154, 2003.

[16] R. Sripriya, N. Suresh, S. Chandra, and D. Bhattacharjee, "The effect of diameter and height of the inserted rod in a dense medium cyclone to suppress air core," *Minerals Engineering*, vol. 42, pp. 1–8, 2013.

[17] Z. Y. Xiong, Z. L. Ji, and X. L. Wu, "Development of a cyclone separator with high efficiency and low pressure drop in axial inlet cyclones," *Powder Technology*, vol. 253, pp. 644–649, 2014.

[18] N. Mikheev, I. Saushin, A. A. Paereliy, D. Kratirov, and K. Levin, "Cyclone separator for gas-liquid mixture with high

flux density," *Powder Technology*, vol. 339, no. 18, pp. 326–333, 2018.

[19] S. Y. Noh, J. E. Heo, S. H. Woo et al., "Performance improvement of a cyclone separator using multiple subsidiary cyclones," *Powder Technology*, vol. 338, no. 18, pp. 145–152, 2018.

[20] I. Karagoz, A. Avci, A. Surmen, and O. Sendogan, "Design and performance evaluation of a new cyclone separator," *Journal of Aerosol Science*, vol. 59, pp. 57–64, 2013.

[21] G. Y. Yu, S. J. Dong, L. N. Yang et al., "Experimental and numerical studies on a new double-stage tandem nesting cyclone," *Chemical Engineering Science*, vol. 236, Article ID 116537, 2021.

[22] J. J. Chen, N. Zhang, Y. W. Yue, and S. Cong, "Dust removal system gas distributor CFD Simulation Optimization," *Modern Chemistry*, vol. 40, pp. 292–299, 2020.

[23] V. Beschkov, E. Razkazova-Velkova, M. Martinov, and S. Stefanov, "Performance of sulfide-driven fuel cell aerated by venturi tube ejector," *Catalysts*, vol. 11, no. 6, p. 694, 2021.

[24] M. G. Rodio and P. M. Congedo, "Robust analysis of cavitating flows in the Venturi tube," *European Journal of Mechanics B: Fluids*, vol. 44, pp. 88–99, 2014.